The Cryosphere Discuss., 6, 4939–4976, 2012
www.the-cryosphere-discuss.net/6/4939/2012/
doi:10.5194/tcd-6-4939-2012

The Cryosphere
Discussions

Evidence and analysis of 2012 Greenland records from spaceborne observations, a regional climate model and reanalysis data

M. Tedesco[1], X. Fettweis[2], T. Mote[3], J. Wahr[4], P. Alexander[1,5], J. Box[6], and B. Wouters[4,7]

[1]The City College of New York, The City University of New York, New York, NY 10031, USA
[2]University of Liege, Liege, Belgium
[3]University of Georgia, Athens, GA 30602, USA
[4]Department of Physics and Cooperative Institute for Research in Environmental Sciences, University of Colorado, Boulder, CO 80309, USA
[5]The Graduate Center of the City University of New York, New York, NY 10031, USA
[6]The Ohio State University, Columbus, OH, USA
[7]School of Geographical Sciences, University of Bristol, Bristol, UK

Received: 24 October 2012 – Accepted: 15 November 2012 – Published: 30 November 2012

Correspondence to: M. Tedesco (mtedesco@sci.ccny.cuny.edu)

Published by Copernicus Publications on behalf of the European Geosciences Union.

Abstract

A combined analysis of remote sensing observations, regional climate model (RCM) outputs and reanalysis data over the Greenland ice sheet provides evidence that multiple records were set during summer 2012. Melt extent was the largest in the satellite era (extending up to ∼ 97 % of the ice sheet) and melting lasted up to ∼ two months longer than the 1979–2011 mean. Model results indicate that near surface temperature was ∼ 3 standard deviations (σ) above the 1958–2011 mean, while surface mass balance was ∼ 3σ below the mean and runoff was 3.9σ above the mean over the same period. Albedo, exposure of bare ice and surface mass balance also set new records, as did the total mass balance with summer and annual mass changes of, respectively, −627 Gt and −574 Gt, 2σ below the 2003–2012 mean.

We identify persistent anticyclonic conditions over Greenland associated with anomalies in the North Atlantic Oscillation (NAO), changes in surface conditions (e.g. albedo) and pre-conditioning of surface properties from recent extreme melting as major driving mechanisms for the 2012 records. Because of self-amplifying positive feedbacks, less positive if not increasingly negative SMB will likely occur should large-scale atmospheric circulation and induced surface characteristics observed over the past decade persist. Since the general circulation models of the Coupled Model Intercomparison Project Phase 5 (CMIP5) do not simulate the abnormal anticyclonic circulation resulting from extremely negative NAO conditions as observed over recent years, contribution to sea level rise projected under different warming scenarios will be underestimated should the trend in NAO summer values continue.

1 Introduction

During the past decade, surface melting over the Greenland Ice Sheet (GrIS) has been increasing (e.g. Fettweis et al., 2012a; Mote, 2007; Tedesco et al., 2008, 2011), with results from regional climate models, in-situ observations and satellite data revealing accelerating ice sheet mass loss (van den Broeke et al., 2009; Rignot et al., 2011). Melting is responsible for summer meltwater production over the GrIS, which can translate into runoff to the surrounding ocean, depending on the evolution of the ice sheet hydrological system. Aside from the direct impact of increased runoff on the surface mass balance (SMB) of the GrIS, changes in the meltwater production affect supraglacial, englacial and subglacial processes. Persistent and enhanced melting can lead to reduced surface albedo (because of snow grain size metamorphism or bare ice exposure, for example) and, consequently, to increased absorbed solar radiation (which further enhances melting). The existence of supraglacial lakes, whose formation is driven by meltwater production, increases the ice ablation rate with respect to the case when ice is exposed to air (e.g. Tedesco et al., 2012a). Moreover, rates of meltwater production play a key role in modulating the opening and persistence of surface-to-bedrock connections (e.g. hydro-fracturing, Weertman, 1973; van der Veen, 2007; Catania et al., 2008), which are associated with ice sheet velocity spatio-temporal gradients and, therefore, can impact the total GrIS mass balance. Given the complex and non-linear nature of the mechanisms linking melting to other surface and sub-surface processes, it is crucial to adopt a multidisciplinary approach in which multiple tools are used to identify different aspects of extreme events and their drivers, allowing to overcome the limitations of a single method to provide a more comprehensive understanding of the phenomenon under observation.

Here we combine results obtained from the analysis of spaceborne remote sensing data, of the outputs of a regional climate model (RCM) and re-analysis data to show evidence that multiple records were set during the summer of 2012 over the GrIS, and to investigate the driving mechanisms. In particular, for the summer of 2012, new records were set for melt extent and duration derived from passive microwave remote sensing (1979–2012), satellite-derived snow/ice surface temperature and albedo (2000–2012), RCM-derived surface mass balance, bare ice exposure, runoff and near-surface temperature (1958–2012), and total mass balance derived from gravimetric satellite measurements (2002–2012). In many cases, the new records were exceeding the mean by values between 2 and 4 standard deviations. In Sect. 2, we describe the data and methods employed; in Sect. 3 we discuss the records associated with each considered data set examined; lastly in Sect. 4, we investigate the drivers of the records; conclusions follow in Sect. 5.

2 Methods and data

2.1 Melt extent and duration from passive microwave data

Wet snow can be mapped at large spatial scales and high temporal resolution from spaceborne measurements collected in the microwave region of the electromagnetic spectrum. As the liquid water content (LWC) within the snowpack increases, so does the absorption as a consequence of the increase of the imaginary part of snow permittivity. In the case of passive microwave sensors, this has the consequence of suddenly and considerably increasing the recorded microwave brightness temperature (Tb). Microwave sensors can also detect sub-surface liquid water, which can occur when the surface is frozen and, therefore, cannot be detected with thermal sensors.

We use data collected by the Scanning Multichannel Microwave Radiometer (SMMR) and by the Special Sensor Microwave Imager (SSM/I). SMMR was a five-frequency instrument on the Nimbus-7 satellite. It had dual-polarised, horizontal (H) and vertical (V), channels at 6.63, 10.69, 18.0, 21.0, and 37.0 GHz (Gloersen et al., 1984). The first SSM/I sensor was launched aboard the DMSP F-8 mission in 1987 (Hollinger et al., 1987). A series of SSM/I sensors on subsequent DMSP satellites has provided a continuous data stream since then. Sensors on the F-8, F-11, F-13, and F-17 platforms are used for the data used here. The SSM/I sensor has seven channels at four frequencies. The 19.4, 37.0, and 85.5 GHz frequencies are dual polarised (H and V); the 22.2 GHz frequency has only a single vertically polarised channel. For simplicity, the channels are sometimes denoted as simply 19H, 19V, 22V, 37H, 37V, 85V and 85H. The SSM/I sensor was replaced by the Special Sensor Microwave Imager/Sounder (SSMIS) sensor with the launch of F-16 in 2003. The SSMIS sensor has the same 19.4, 22.2, and 37.0 GHz channels of SSM/I; however, the 85.5 GHz channels on SSM/I are replaced with 91.0 GHz channels on SSMIS. This does not affect the melt detection, as this frequency is not used in the algorithms considered here.

The National Snow and Ice Data Center (NSIDC) processes and combines swath brightness temperature data from Remote Sensing Systems, Inc. (RSS) (http://www.ssmi.com). The NSIDC distributes SMMR, SSM/I and SSMIS as gridded daily products, distributed in a polar stereographic projection and the Equal-Area Earth Scalable (EASE) projection with a 25 km spatial resolution. Near-real time DMSP SSMIS daily polar gridded brightness temperatures (http://nsidc.org/data/nsidc-0080.html) and EASE-Grid brightness temperatures (http://nsidc.org/data/docs/daac/nsidc_0342_nrt_ssmi_ease_tb) are also available through NSIDC and are used here for the analysis reported in the following for the 2012 season. Though near-real time data did not go through the same processing as fully processed data, the difference between the two data sets is generally small (on the order of 1–2 K at the maximum but below that on the average based on a comparison performed by the authors using data from previous years over the Greenland ice sheet). Because of the strong impact of LWC on recorded brightness temperatures (e.g. increase of the order of tens of K, up to 100 K in some cases, when moving from dry to wet snow conditions, e.g. Tedesco, 2007), we assume that the use of near-real time brightness temperatures does not impact the results discussed in the following for the 2012 melting season.

Changes in melt duration and extent over the Greenland and Antarctic ice sheets have been mapped using the seasonal change in emissivity and thresholds computed through the aid of electromagnetic models (Mote and Anderson, 1995; Mote, 2007; Tedesco, 2009), the frequency dependence of emissivity, such as the cross polarised gradient ratio (XPGR, e.g. Abdalati and Steffen, 1997; Steffen et al., 2004), the diurnal change in emissivity (e.g. Tedesco, 2007) and fixed threshold coefficients (e.g. Zwally and Fiegles, 1994). Here, we use the algorithms reported by Mote and Anderson (1995) and Tedesco (2009), as they are based on a similar concept (e.g. when the LWC within the snowpack is assumed to exceed a certain threshold). The algorithm of Mote and Anderson (1995) is a dynamic threshold algorithm (DTA) based on a simple microwave-emission model, which is used to simulate 37 GHz, horizontally polarised brightness temperatures associated with 1 % liquid water content across the Greenland ice sheet (Mote, 2007). The other approach is based on Tedesco (2009) and assumes a fixed value of LWC to compute the brightness temperature threshold (still from an electromagnetic model) above which melt is assumed to be occurring. This approach is conceptually similar to the one originally proposed by Zwally and Fiegles (1994), producing coefficients that are similar to those produced in that approach but that are spatially and temporally dynamically computed.

2.2 MODIS albedo and surface temperature

The Moderate-resolution Imaging Spectroradiometer (MODIS) on board the Terra and Aqua satellites (http://modis.gsfc.nasa.gov/) records data in 36 spectral bands between 0.4 and 14.4 µm. MODIS thermal infrared observations allow estimates of land surface temperature (LST) under cloud-free conditions at a 1 km horizontal spatial resolution. In particular, the MODIS MOD11A1 data product (http://www.icess.ucsb.edu/modis/LstUsrGuide/usrguide_1dtil.html) makes use of daily averaged LST retrievals from swath data using bands 31 (11 µm) and 32 (12 µm) (Wan et al., 2002; Wan, 2008). The root mean square error (RMSE) of the MOD11A1 product, with respect to independent in-situ observations, has been estimated to be 1 °C (Wan, 2008), with higher RMS errors (> 1 °C) found over Greenland (Hall et al., 2008a,b; Koenig and Hall, 2010).

Surface albedo retrievals from the NASA Terra platform MODIS sensor beginning 5 March 2000 are available from the NSIDC (Hall et al., 2011). The daily MOD10A1 product is used in this study instead of other available products, such as the MODIS MOD43 (http://modis.gsfc.nasa.gov/data/dataprod/dataproducts.php?MOD_NUMBER=43) or MCD43 8-day (http://www-modis.bu.edu/brdf/userguide/intro.html) products, in order to increase temporal resolution. After collection, the data are interpolated to a 5 km EASE grid. Stroeve et al. (2006) showed that the MOD10A1 product captures the albedo seasonal cycle, but exhibits more temporal variability than recorded by in-situ observations. A dominant component of this assessed error might be the failure of the MODIS data product to completely remove cloud effects. Another problem might be the presence of spuriously low values, for example below 0.4 in the accumulation area, where albedo is not observed by pyranometers at the surface to drop below 0.7. In this study, we follow the approach reported by Box et al. (2012), in which 11-day running statistics are here used to identify and reject values that exceed 2 standard deviations from an 11-day average. To prevent rejecting potentially valid cases, data within 0.04 of the median are not rejected. June–August (JJA or summer) seasonal averages are then generated from monthly averages of the daily filtered and smoothed data. Only data from the Terra MODIS instrument is used in this study, to reduce computational burdens, and given an Aqua MODIS instrument near infrared (channel 6) failure (Hall et al., 2008a) that reduces the cloud detection capability.

2.3 The MAR regional climate model

MAR is a three-dimensional coupled atmosphere-land surface model that predicts the evolution of the coupled land-atmosphere system (subject to land-atmosphere feedbacks) in response to radiative forcing from the sun, and known or projected atmospheric forcing applied at the model's lateral boundaries. The atmospheric portion of MAR is coupled to the 1-D Surface Vegetation Atmosphere Transfer scheme SISVAT (Soil Ice Snow Vegetation Atmosphere Transfer, Gallée and Schayes (1994) and De Ridder and Gallée, 1998), which simulates surface properties and the exchange of mass and energy between the surface and the atmosphere. SISVAT incorporates an interactive snow model based on the CROCUS model (Brun et al., 1992): a 1-D layered energy and mass balance model of the snowpack. CROCUS is more sophisticated with respect to snow models used by most RCMs (e.g. Rae et al., 2012) in that it is a physically based model capable of simulating the evolution of snow properties, such as grain sizes and shapes, in response to energy and mass changes within the snowpack, and their influence on surface albedo. CROCUS also incorporates a water balance module that takes into account the re-freezing of meltwater, a turbulence module, and a snow/ice discretisation module (Brun et al., 1992).

MAR has been used to simulate long-term changes in the GrIS SMB and surface melt extent (Fettweis et al., 2005, 2011; Tedesco et al., 2008, 2011) using ERA-40 (1958–1978) and ERA-INTERIM reanalysis (1979–2012) as forcing every 6 h at the MAR lateral boundaries. Validation has been performed through comparison with ground measurements (e.g. Lefebre et al., 2003, 2005; Gallée et al., 2005), and satellite data (e.g. Fettweis et al., 2005, 2011; Tedesco et al., 2011). These studies have demonstrated the validity of the model for accurately simulating climate changes (Fettweis et al., 2012b; Franco et al., 2012b) and capturing feedback mechanisms, including surface air temperatures, specific humidity, wind speed, surface albedo, melting, and radiative fluxes over Greenland. Here, MAR is run at a 25 km resolution (though outputs can be used to estimate the SMB at higher resolution, e.g. Franco et al., 2012a) with the specific model setup discussed by Fettweis (2007) and with adjustments to the albedo scheme as noted by Fettweis et al. (2011).

2.4 GRACE

The Gravity Recovery and Climate Experiment (GRACE) satellite mission has been providing monthly solutions for the Earth's global gravity field since its launch in spring of 2002. These solutions can be used to determine time variations in the gravity field, which provide information on month-to-month variations in the Earth's mass distribution (e.g. Tapley et al., 2004; Wahr et al., 2004). Here, we use monthly GRACE gravity fields from April, 2002 through September, 2012, generated and made publicly available by the Center for Space Research (CSR) at the University of Texas (http://podaac.jpl.nasa.gov/grace), to solve for temporal changes in the total mass of the Greenland ice sheet. CSR's Release 4 fields were used for months prior to March 2003, and Release 5 fields were used for all months thereafter. Each monthly field consists of a set of spherical harmonic geoid coefficients up to degree and order 60. We replace the GRACE C_{20} coefficients with C_{20} coefficients inferred from satellite laser ranging (Cheng and Tapley, 2004), and we include degree-one coefficients computed as described by Swenson et al. (2007) (coefficients provided by S. Swenson). We use model results from A et al. (2012) to remove contributions from glacial-isostatic-adjustment (GIA): the Earth's viscoelastic response to past ice mass variability. Those GIA results were computed for a compressible, spherically symmetric Earth, and were based on the global ICE-5G model and VM2 viscosity profile of Peltier (2004).

We compute the temporal mean of the monthly fields and subtract that mean from each field, so that the residuals represent the monthly departures from the mean. We convolve each monthly residual field with a Greenland averaging kernel, as described by Velicogna and Wahr (2006), to obtain an estimate of Greenland mass-per-area in units of cm of water, averaged over the ice sheet. Because any such convolution causes a loss of signal, we multiply each monthly mass-per-area estimate by a scaling factor to obtain variations in the total mass of the ice sheet (in Gt) about its temporal average. The scaling factor is computed as described by Velicogna and Wahr (2006), and is determined by applying this analysis procedure to several simulated, but plausible, ice loss patterns.

3 Results

3.1 Surface temperature

Figure 1a shows the map of 2012 JJA near-surface air temperature (3 m) anomalies (1958–2011 baseline) from MAR, indicating largely positive anomalies (up to +4 °C–5 °C) over the entire GrIS. Surface temperature anomalies are extreme at high elevations, especially in the north and south regions, where melting lasted longer than previous years (see next section). Anomalies at relatively low elevations closer to the coast are $\sim 0\,^{\circ}$C. This is a consequence of the fact that melting generally occurs there every year for most of the summer and, therefore, near-surface air temperature is already close to the melting point for most of the season. Figure 1b shows the mean JJA

LST estimated by MODIS averaged over the entire Greenland ice sheet for the period 2000–2012. The JJA ice-sheet-wide MODIS LST increased 3.4 °C between years 2000 and 2012, from an average value of ∼ −9 °C in 2000 to −5.6 °C in 2012, with a linear fit suggesting an increase of +2.1 ± 0.7 °C over the 13 last years. The MAR model suggests an increase of +1.4 °C of the JJA near-surface temperature for the period 2000–2012. The 2012 JJA average GrIS near-surface temperature simulated by MAR was the warmest since 1958, with an anomaly of +2.6 °C (i.e. 2.9 times the standard deviation over 1958–2011). Finally, some coastal weather stations recorded JJA 2012 as the warmest JJA period since the beginning of the observations (more than 100 yr) according to Hanna et al. (2012a). We note that while MODIS provides estimates of the actual snow/ice surface temperature, the near-surface air temperature represents the air temperature at 3 m above the surface.

3.2 Melting from passive microwave spaceborne data

Melting in 2012 set a new record, according to results obtained from spaceborne microwave data (Tedesco, 2009; Mote and Anderson, 1995). Nearly the entire 2012 summer experienced above-normal melt extent across the ice sheet (Fig. 2a). The only multiple-day periods with below-average melt extent occurred between 10–24 May and at the end of August. Apart from a period around mid-June, more extensive melt than average persisted from 27 May through 22 July and throughout much of August 2012. The area covered by melting was larger in 2012 than for any other year in the microwave satellite era (1979–2012), and 2012 was the first year within the satellite era when nearly the entire ice sheet experienced melt (Fig. 2b). The melt extent on Greenland reached a one-day record during the period 11–12 July, when at least 97 % of the ice sheet underwent melt (Nghiem et al., 2012), and more than tripled the 1981–2010 average for 11–12 July (23 %, based on Mote and Anderson, 1995). The 2012-updated trend for melt extent is 22 337 ± 24 $\text{km}^2\,\text{yr}^{-1}$ following Mote and Anderson (1995) and 20 325 ± 22 $\text{km}^2\,\text{yr}^{-1}$ following Tedesco (2009).

In 2012, melting started more than two weeks earlier than average along large bands of the ice sheet below 1200 m a.s.l. An analysis updated through summer 2012 indicates that areas below 2400 m a.s.l. have experienced increasingly earlier melt onset dates since 1979, with the greatest changes occurring at lower elevations (Fig. 3, Table 1). According to results obtained using the algorithm of Mote and Anderson (1995), melt onset at the lowest elevations (< 400 m.a.s.l.) has been occurring 11.59 days earlier per decade ($r = 0.78$). This implies that, on average, melting in 2012 started about one month earlier than it did 33 yr ago. At higher elevations, as expected, the trend of the melt onset is smaller, with melting starting on average 2.65 days earlier per decade ($r = 0.23$) for areas above 2400 m and below 2800 m (areas above 2800 m are not considered here because they do not melt every year). The regression coefficient of the melt onset trend expressed as a function of elevation is 0.0368 ± 0.0004 days m^{-1} decade^{-1} ($r = 0.97$). Before 2012 the trend of the melt onset regression coefficients was 0.0360 ± 0.0004 days m^{-1} decade^{-1}. Similar values are obtained using the melt detection algorithm of Tedesco (2009).

In 2012, melting lasted longer than average for the majority of the areas subject to melting (Figs. 4a, b), up to 30 days longer than the 1981–2010 average for large areas of West Greenland below 2400 m a.s.l. For areas in northwest Greenland between 1400 and 2000 m a.s.l., melting lasted up to two months longer than average. The cumulative melting index, MI (e.g. defined as the number of melting days times the area subject to melting), set a new record in 2012. Figure 4c shows the time series of the annual standardized melting index (SMI, the MI minus its mean and divided by the standard deviation) obtained using the results from the two passive microwave algorithms. The new SMI record was ~ 2.5 standard deviations above the 1981–2010 mean (represented by the 0 value on the y-axis in the SMI plot), while the previous record set in 2010 was ~ 1.2 standard deviations above the mean.

Because the use of microwave data does not allow one to estimate either LWC within the snowpack (or ice) or the amount of liquid water that refreezes after melting, it is difficult to translate the surface melting record detected by spaceborne microwave sensors

Title Page
Abstract Introduction
Conclusions References
Tables Figures
◀| |▶
◀ ▶
Back Close
Full Screen / Esc
Printer-friendly Version
Interactive Discussion

into runoff and, ultimately, into surface mass balance. Moreover, to interpret the 2012 melting record in terms of surface mass balance, it is essential to know the mass that accumulated after the end of the previous melting season and to compute the net mass for the hydrological year (which here is defined starting on 1 September and ending on 31 August). To this aim, the results of the regional climate model MAR are used here to complement those obtained from remote sensing and are reported in the following section.

3.3 Surface mass balance

The SMB simulated by MAR for the 2011–2012 hydrological year (from September 2011 through August 2012) is the lowest for the period 1958–2012 (Fig. 5a, $\sim -400\,\mathrm{Gt\,yr^{-1}}$ anomaly), setting a new record for modelled SMB. The 2012 SMB value is 3 standard deviations below the 1958–2011 mean, exceeding by $\sim 100\,\mathrm{Gt\,yr^{-1}}$ the previous record set in 2010 ($\sim -300\,\mathrm{Gt\,yr^{-1}}$ anomaly, Fig. 5a). According to MAR, the 2012 SMB record is driven by the record melt and the associated modelled runoff ($\sim 350\,\mathrm{Gt\,yr^{-1}}$, 3.9 standard deviations above the 1958–2011 average). The simulated winter snowfall over 2011–2012 does not play a major role in setting the SMB record, because it is close to the 1958–2011 average. This is different from previous record melt summers (2007, 2008, 2010, 2011), when the low SMB anomaly was driven by substantial contributions from both high runoff anomalies and reduced winter accumulation (Tedesco et al., 2011). Figure 5b shows the daily time series of the cumulative SMB for 2010, 2011 and 2012, as well as for the 1958–2011 mean. The graph shows that the accumulated mass during winter in the case of 2010 was lower than that in 2011 and 2012 and highlights the relatively steep slope of the cumulative SMB starting around day 192 (10 July) 2012 (linear regression between day 192 and day 246 of $-7.69 \pm 0.2\,\mathrm{Gt\,yr^{-1}\,day^{-1}}$, $R^2 = 0.99$) with respect to 2011 ($-5.4 \pm 0.2\,\mathrm{Gt\,yr^{-1}\,day^{-1}}$) and 2010 ($-5.15 \pm 0.13\,\mathrm{Gt\,yr^{-1}\,day^{-1}}$). Figure 6a shows the map of SMB anomalies for the 2011–2012 hydrological year simulated by MAR. SMB was below the average over the entire ice sheet with relatively low values in the ablation zone of the west and southeast regions. Simulated meltwater production for June through August (JJA, Fig. 6b) was also above the average over the entire ice sheet, with relatively high values (e.g. between 200 and 400 mm WE yr^{-1}) at high elevations in South Greenland. Snowfall was considerably lower than normal in South Greenland for the JJA period of 2012 (Fig. 6c), as a result of abnormal anticyclonic conditions (discussed later). This quasi-absence of snowfall during summer (combined with more sunny conditions than normal resulting from the position of the anticyclone) was likely responsible for maintaining a low albedo during the entire summer in Southern Greenland, further enhancing melting in this area. The reduced snowfall in the southeast is also due to the fact that a larger part of precipitation in the summer of 2012 fell as rainfall rather than as snowfall (not shown here), due to warmer conditions.

3.4 Albedo

MODIS results indicate that the ice-sheet-wide average albedo for JJA 2012 was the lowest since MODIS began collecting data with a value of 0.684 (vs. a value of 0.750 in year 2000), decreasing by 6.6 % between 2000 and 2012 and with a linear fit suggesting a -6.4 ± 0.8 % change. The degrading MODIS instrument sensitivity identified by Wang et al. (2012) introduces the possibility that the declining albedo trends may be erroneous. However, Box et al. (2012) ruled out this problem through comparison of the MOD10A1 data with ground observations from sites distributed around the ice sheet and spanning 11 yr. Figure 7a–c shows the MODIS daily albedo anomaly map for 19 July (a), 3 August (b) and 23 August 2012 (c) with respect to the 2000–2011 mean for the same days obtained from MODIS. Figure 7d shows the 2012 JJA albedo anomaly (with respect to the 1979–2011 baseline) obtained from MAR. Differences between the two maps can be attributed to the intrinsic differences between the two approaches, to the different baseline periods, and the spatial resolution of the two data sets. Nevertheless, both maps consistently indicate a decrease in albedo in 2012 with respect to previous years, especially along the southwest coast of Greenland. The time series of the 2012 albedo simulated by MAR, together with the 1958–2011 mean and the absolute daily minimum albedo over the 1958–2011 period, are plotted in Fig. 7e. MAR suggests that in 2012, the albedo over Greenland was below average, reaching new record low values in July and experiencing close-to-record values for most of August, with the exception of a short period at the beginning of August after a snowfall event.

3.5 Total mass change from GRACE

Results from GRACE reveal record 2012 GrIS mass loss, occurring in concert with the record observed and modelled surface temperature, albedo, and SMB anomalies indicated above. Figure 8 shows the cumulative mass anomalies (CMA) from GRACE through September 2012 over Greenland. The differences between the September and June CMA values and September through September are reported in Table 2. GRACE did not deliver a June value in 2003 or 2011. For those years, we used the May value instead, but we modified that value by adding the average difference (13 ± 40 Gt, where ±40 is a 2σ uncertainty estimate) between June and May for the 8 yr (2004–2010, and 2012) in which both values were given. The error on the summer CMA results are computed by smoothing the monthly CMA values, subtracting that difference from the unsmoothed values, and computing the 2σ scatter of the residuals. Figure 8 and Table 2 show that when compared with all years during 2003–2012, 2012 set new records in terms of summertime and annual mass loss, with a mass change between June and August of −627 ± 89 Gt, approximately 2σ below the 2003–2012 mean of −414 Gt. The previous record was set in 2010, with a summer CMA value of −516 ± 89 Gt, which lays $\sim 0.8\sigma$ below the mean. The summer mass change values have been growing steadily more negative over the GRACE period of observation. The trend of those values during 2003–2012 is $-29 \pm 11\,\mathrm{Gt\,yr^{-1}}$. That trend reduces to $-20 \pm 13\,\mathrm{Gt\,yr^{-1}}$ if the summer of 2012 is excluded, which is a consequence of the fact that the 2012 summer mass loss was anomalously large, even after factoring in the steady increase in summer mass loss that has been occurring in recent years. In terms of annual loss (e.g. from mid-September to the successive mid-September) the 2012 loss was −575 ± 89 Gt ($\sim 2\sigma$

below the mean), also setting a new record, exceeding the previous record set in 2010 of −423 ± 89 Gt ($\sim 0.7\sigma$ below the mean).

4 Discussion

The analysis of both modelling and satellite data (Figs. 2a and 6d) indicates that the 2012 melt season started at the end of May with a warm event that was not enough to completely remove the 2011–2012 winter accumulation in the ablation area, with the modelled bare ice exposed area remained relatively low (see Fig. 9). From mid-June to the beginning of July, there was a succession of warm episodes that increased melting and decreased albedo, but large areas in the ablation area still remained covered by the winter snowpack. Around 10 July, an anticyclonic ridge inducing one of the warmest conditions over the past 50 yr contributed to the melting of most of the winter accumulation, exposing large bare ice regions in the ablation zone (seen as an increase in bare ice in Fig. 9). This event reduced the ice sheet albedo (Fig. 7c) and induced the highest daily-modelled meltwater production in the past 50 yr (Fig. 6d). A fourth melt event occurred at the end of July 2012, melting the fresh snow accumulated around 20 July and favouring the reduction in the albedo again. In general, the reduction of the albedo can be attributed to grain size metamorphism (e.g. constructive metamorphism reduces albedo through bounding of smaller grains) as well as bare ice exposure and ablation area melt water ponding. From Fig. 7a–d it is possible to observe that low negative albedo anomalies occur along the coastal areas corresponding to those regions where bare ice was exposed. In addition to the time series of the 2012 bare ice exposed area simulated by MAR, Fig. 9 shows the 1958–2011 mean and the absolute daily maximum bare ice area over 1958–2011. A comparison between Figs. 9 and 7e reveals a clear relationship between the MAR modelled albedo reduction for July and August and the simulated increase of the bare ice area exposed. This is the consequence of the increased melting on one side, but also of the reduced solid precipitation along Southwest Greenland that characterised summer 2012 (as a consequence of the discussed anticyclonic, e.g. dry and warm, conditions).

In a synthetic sensitivity experiment, we tested the hypothesis that the simulated record of bare ice exposure might have been pre-conditioned by previous recent melting record years (e.g. 2010 and 2011). The removal of the seasonal accumulation from the previous years might indeed allow a premature exposure of bare ice, once the 2011–2012 winter accumulation melted in June 2012. We replaced MAR snowpack state variables for the top 10 m (density, temperature, grain size, etc.) on 1 May 2012 with those from 1 May 1997 (when previous summers were particularly wet and cold). The results of those simulations obtained using the May 1997 snowpack conditions are reported as green lines in Figs. 6d, 7c and 9. The outputs indicate that with these new initial conditions for the snowpack (e.g. May 1997) the run-off rate (resp. meltwater production) is reduced by 20 % (resp. by 10 %) compared to the case when the original snow conditions from May 2012 were used. The decrease in run-off is greater because run-off of meltwater occurs mainly above the bare ice area. These results indicate that pre-conditioning of the snowpack from previous years contributed to the record melt events of 2012.

Melting in 2012 was also considerably higher than normal along the western GrIS coast as a result of the enhanced warm southerly air advection associated with the abnormal persistence of anticyclonic circulation centred in South Greenland. Figure 10 shows an anticyclonic-like anomaly at 700 hPa in the geopotential height (Z700) for JJA 2012 occurring mainly over Greenland, which is not manifest over other regions of the Arctic, indicating a local pattern associated to the North Atlantic Oscillation (NAO). Following Fettweis et al. (2012a), we classified 16 % of the JJA days for 2012 as low pressure-like days, 55 % as anticyclonic days and 28 % as day with a general circulation over Greenland similar to the JJA climatological mean. On average over the period 1958–2011, the NCEP-NCAR reanalysis data shows that summer has, respectively, about 30 ± 12 %, 20 ± 10 % and 50 ± 10 % as low pressure like days, anticyclonic and normal days. The identified frequency of the JJA days classified as anticyclonic during summer is the highest in 50 yr (e.g. 2007: 40 %, 2010: 33 %, 2011: 47 %). Figure 3 of Fettweis et al. (2012a) shows the corresponding 500 hPa geopotential height for the three types of circulation as well as the temperature anomalies at 700 hPa induced by these circulation types. As shown in that figure, the JJA run-off amount simulated by MAR (forced by the ECMWF reanalysis) is highly correlated to the JJA mean temperature at 700 hPa (T700) over Greenland. As for melt, T700 in Summer 2012 was the highest in the previous 50 yr. Daily analogues JJA circulations taken over 1961–1990 explain 55 ± 5 % of the T700 anomaly in 2012. We refer to Fettweis et al. (2012a) for more details about the analogue flows methodology and why 1961–1990 is chosen here as a baseline period. The analysis suggests that the abnormal anticyclonic conditions of summer 2012 explain at least 55 % of this summer's T700 anomaly, and ultimately surface melt. The remaining 45 % might be, therefore, attributed to a more general long-term warming occurring in the Arctic, resulting in part from a global warming, as discussed by Fettweis et al. (2012a).

The persistent anomalous ridging over Greenland was associated with persistent and anomalously negative North Atlantic Oscillation (NAO) index values. The NAO is the leading mode of low frequency variability in the cool season across the North Atlantic and is a large-scale dipole in atmospheric mass between the subtropical high and the polar low. Negative NAO values are associated with higher pressure and temperature over Greenland (Thompson and Wallace, 1998), surface melt extent (Mote, 1998; Tedesco et al., 2011), and melt/runoff (Hanna et al., 2012a). Negative NAO values have been persistent during summers since 2006, but the summer of 2012 featured the most negative NAO for the period 1950–2012 (Fig. 11), based on the NOAA Climate Prediction Center NAO index values (Barnston and Livezey, 1987).

5 Conclusions

Relative to the beginning of the satellite record in 1979, melting in Greenland is now starting about one month earlier at low elevations, with the area subject to melting increasing over 1979–2012 at a rate of between ~20 000 and 22 000 $\mathrm{km^2\,yr^{-1}}$ (depending on the algorithm used). The amount and duration of melting at higher elevations has also been increasing, though at a slower rate. In this context, 2012 set new records in terms of melt extent (up to ~97 % of the entire ice sheet) and duration (up to about two months above the 1979–2012 mean for some areas), albedo, modelled bare ice exposure, SMB and runoff, and overall mass loss. The 2012 SMB anomaly (1958–2011 baseline) was ~ −400 $\mathrm{Gt\,yr^{-1}}$ and the runoff anomaly was 350 $\mathrm{Gt\,yr^{-1}}$. The cumulative mass anomaly from GRACE indicates values of ~ −627 Gt for the summer period and −574 Gt for the 2012 hydrological year. These anomalies exceed the record anomalies of 2010, when SMB and runoff records were also set.

Premature and longer bare ice exposure was responsible, together with positive surface temperature anomalies, for the enhanced melting, which drove the SMB record in 2012. Bare ice exposure was pre-conditioned by previous record melting years, through the removal of seasonal snowpack accumulated during the previous years. Should the trend continue for melting, there will be more bare ice exposed sooner and for longer periods, reducing surface albedo and leading to more absorbed solar energy. Moreover, anticyclonic conditions observed in recent years persisted in 2012, supporting more melting through the reduction of summer solid precipitation, persistent clear-sky conditions and the advection of warm air from the south with the role played by the oceanic summer conditions around Greenland appearing to be negligible relative to the effects of the general circulation patterns (Hanna et al., 2012b).

Large scale circulation patterns (e.g. NAO) and changes in local conditions have acted in concert to increase SMB losses over previous years, through reduction of snowfall, increasing liquid precipitation and runoff. Because of positive feedbacks such as the albedo feedback, more negative SMB will likely occur should large-scale atmospheric circulation characteristics observed over the past decade persist. Surface mass loss, together with losses from glacial flow, have been driving the recent records in terms of total mass loss identified through GRACE. Drainage basins along the southwest coast are projected to have the highest sensitivity of SMB to increasing temperatures during the 21st century (Tedesco and Fettweis, 2012; Fettweis et al., 2012b). For these basins, the global temperature anomaly corresponding to a decrease of the SMB below the 1980–1999 average (when the ice sheet was near equilibrium) ranges between +0.60 °C and +2.16 °C (Tedesco and Fettweis, 2012). These are also the basins where positive feedbacks associated with bare ice exposure are projected to be the strongest. Recent studies have pointed to persistent changes in early summer Arctic wind patterns relative to previous decades, suggesting an enhancement of the so-called Arctic Dipole (AD), enhanced meridional flow across the Arctic for the period 2007–2012 and an increase in the Greenland Blocking Index (GBI, e.g. Overland et al., 2012), suggesting overall changes in atmospheric circulation. Because the CMIP5 general circulation models, used to predict future climate changes, do not project changes of the general circulation in summer over Greenland through this century (Belleflamme et al., 2012; Fettweis et al., 2012a), their outputs do not account for the abnormal anticyclonic circulation resulting from negative NAO conditions that have been observed in recent years and that have been partially driving the enhanced melting and the observed records. Moreover, the MAR model and other RCMs, which have been used to project future SMB changes (e.g. Tedesco and Fettweis, 2012), are not currently coupled with ice sheet flow models and, consequently, the impact of increased melting on ice dynamics is not accounted for. This suggests that the projected contribution to sea level rise under different warming scenarios might be underestimated (and the sensitivity to temperature changes might be higher) and points to the need for a synergic continuous monitoring of current changes using multiple tools (e.g. field observations, remote sensing, modelling) and interdisciplinary fields (e.g. a merging of glaciology, hydrology, atmospheric science) to improve future projections of the evolution of the GrIS.

Acknowledgements. M.T. and P.A. acknowledge the support of the NSF through grant # 0909388 and of the NASA Cryospheric Sciences Program. B.W. is funded by a Marie Curie International Outgoing Fellowship within the 7th European Community Framework Programme (FP7-PEOPLE-2011-IOF-301260). J. W.'s contributions were partially supported by NASA grant NNX08AF02G and NNXI0AR66G, and by NASA's "Making Earth Science Data Records for Use in Research Environments (MEaSUREs) Program".

References

A, G., Wahr, J., and Zhong, S.: Computations of the viscoelastic response of a 3-D compressible Earth to surface loading: an application to Glacial Isostatic Adjustment in Antarctica and Canada, Geophys. J. Int., in press, 2012.

Abdalati, W. and Steffen, K.: Snowmelt on the Greenland ice sheet as derived from passive microwave satellite data, J. Climate, 10, 165–175, 1997.

Barnston, A. G. and Livezey, R. E.: Classification, seasonality and persistence of low-frequency atmospheric circulation patterns, Mon. Weather Rev., 115, 1083–1126, 1987.

Belleflamme, A., Fettweis, X., Lang, C., and Erpicum, M.: Current and future atmospheric circulation at 500 hPa over Greenland simulated by CMIP3 and CMIP5 global models, Clim. Dynam., submitted, 2012.

Box, J. E., Fettweis, X., Stroeve, J. C., Tedesco, M., Hall, D. K., and Steffen, K.: Greenland ice sheet albedo feedback: thermodynamics and atmospheric drivers, The Cryosphere, 6, 821–839, doi:10.5194/tc-6-821-2012, 2012.

Brun, E., David, P., Sudul, M., and Brunot, G.: A numerical model to simulate snow-cover stratigraphy for operational avalanche forecasting, J. Glaciol., 38, 13–22, 1992.

Catania, G. A., Neumann, T. A., and Price, S. F.: Characterizing englacial drainage in the ablation zone of the Greenland ice sheet, J. Glaciol., 54, 567–578, 2008.

Cheng, M. and Tapley, B. D.: Variations in the Earth's oblateness during the past 28 yr, J. Geophys. Res., 109, B09402, doi:10.1029/2004JB003028, 2004.

De Ridder, K. and Gallée, H.: Land surface-induced regional climate change in Southern Israel, J. Appl. Meteorol., 37, 1470–1485, 1998.

Fettweis, X.: Reconstruction of the 1979–2006 Greenland ice sheet surface mass balance using the regional climate model MAR, The Cryosphere, 1, 21–40, doi:10.5194/tc-1-21-2007, 2007.

Fettweis, X., Gallée, H., Lefebre, F., and van Ypersele, J.-P.: Greenland surface mass balance simulated by a regional climate model and comparison with satellite-derived data in 1990–1991. Clim. Dynam., 24, 623–640, doi:10.1007/s00382-005-0010-y, 2005.

Fettweis, X., Tedesco, M., van den Broeke, M., and Ettema, J.: Melting trends over the Greenland ice sheet (1958–2009) from spaceborne microwave data and regional climate models, The Cryosphere, 5, 359–375, doi:10.5194/tc-5-359-2011, 2011.

Fettweis, X., Hanna, E., Lang, C., Belleflamme, A., Erpicum, M., and Gallée, H.: Brief communication “Important role of the mid-tropospheric atmospheric circulation in the recent surface melt increase over the Greenland ice sheet”, The Cryosphere Discuss., 6, 4101–4122, doi:10.5194/tcd-6-4101-2012, 2012a.

Fettweis, X., Franco, B., Tedesco, M., van Angelen, J. H., Lenaerts, J. T. M., van den Broeke, M. R., and Gallée, H.: Estimating Greenland ice sheet surface mass balance contribution to future sea level rise using the regional atmospheric climate model MAR, The Cryosphere Discuss., 6, 3101–3147, doi:10.5194/tcd-6-3101-2012, 2012b.

Franco, B., Fettweis, X., Lang, C., and Erpicum, M.: Impact of spatial resolution on the modelling of the Greenland ice sheet surface mass balance between 1990–2010, using the regional climate model MAR, The Cryosphere, 6, 695–711, doi:10.5194/tc-6-695-2012, 2012a.

Franco, B., Fettweis, X., and Erpicum, M.: Future projections of the Greenland ice sheet energy balance driving the surface melt, developed using the regional climate MAR model, The Cryosphere Discuss., 6, 2265–2303, doi:10.5194/tcd-6-2265-2012, 2012b.

Gallée, H. and Schayes, G.: Development of a three-dimensional meso-γ primitive equation model: katabatic winds simulation in the area of Terra Nova Bay, Antarctica, Mon. Weather. Rev., 122, 671–685, 1994.

Gallée H., Peyaud V., and Goodwin, I.: Simulation of the net snow accumulation along the Wilkes Land transect, Antarctica, with a regional climate model, Ann. Glaciol., 41, 17–22, 2005.

Gloersen, P., Cavalieri, D. J., Chang, A. T. C., Wilheit, T. T., Campbell, W. J., Johannessen, O. M., Katsaros, K. B., Kunzi, K. F., Ross, D. B., Staelin, D., Windsor, E. P. L., Barath, F. T., Gudmandsen, P., Langham E., and Ramseier, R. O.: A summary of results from the first NIMBUS-7 SMMR observations, J. Geophys. Res., 89, 5335–5344, 1984.

Hanna, E., Jones, J. M., Cappelen, J., Mernild, S. H., Wood, L., Steffen, K., and Huybrechts, P.: The influence of North Atlantic atmospheric and oceanic forcing effects on 1900–2010 Greenland summer climate and ice melt/runoff, Int. J. Climatol., doi:10.1002/joc.3475, 2012a.

Hanna, E., Fettweis, X., Mernild, S. H., Cappelen, J., Ribergaard, M., Shuman, C., Steffen, K., Wood, L., and Mote, T.: Atmospheric and oceanic climate forcing of the exceptional Greenland ice sheet surface melt in summer, J. Climate, in preparation, 2012b.

Hollinger, J., Lo, R., Poe, G., Savage, R., and Pierce J.: Special Sensor Microwave/Imager User's Guide, Naval Research Laboratory Report, Washington, DC, 1987.

Hall, D. K., Williams Jr., R. S., Luthcke, S. B., and Digirolamo, N. E.: Greenland ice sheet surface temperature, melt and mass loss: 2000–2006, J. Glaciol., 54, 81–93, doi:10.3189/002214308784409170, 2008a.

Hall, D. K., Box, J. E., Casey, K., Hook, S. J., Shuman, C. A., and Steffen, K.: Comparison of satellite-derived and in-situ observations of ice and snow surface temperatures over Greenland, Remote. Sens. Environ., 112, 3739–3749, 2008b.

Hall, D. K., Riggs, G. A., and Salomonson, V. V.: MODIS/Terra Snow Cover Daily L3 Global 500 m Grid Version 4, January to March 2003, Digital media, updated daily, National Snow and Ice Data Center, Boulder, CO, USA, 2011.

Koenig, L. S. and Hall, D. K.: Comparison of satellite, thermochron and air temperatures at summit, Greenland, during the winter of 2008/09, J. Glaciol., 56, 735–741, 2010.

Lefebre, F., Gallée, H., van Ypersele, J.-P., and Greuell, W.: Modeling of snow and ice melt at ETH Camp (West Greenland): a study of surface albedo. J. Geophys. Res., 108, 4231, doi:10.1029/2001JD001160, 2003.

Lefebre, F., Fettweis, X., Galée, H., van Ypersele, J.-P., Marbaix, P., Greuell, W., and Calanca, P.: Evaluation of a high-resolution regional climate simulation over Greenland, Clim. Dynam., 25, 99–116, doi:10.1007/s00382-005-0005-8, 2005.

Mote, T. L.: Mid-tropospheric circulation and surface melt on the Greenland ice sheet, Part I: Atmospheric teleconnections, Int. J. Climatol., 18, 111–129, 1998.

Mote, T. L.: Greenland surface melt trends 1973–2007: evidence of a large increase in 2007, Geophys. Res. Lett., 34, L22507, doi:10.1029/2007GL031976, 2007.

Mote, T. L. and Anderson, M. R.: Variations in melt on the Greenland ice sheet based on passive microwave measurements, J. Glaciol., 41, 51–60, 1995.

Nghiem, S. V., Hall, D. K., Mote, T. L., Tedesco, M., Albert, M. R., Keegan, K., Shuman, C. A., DiGirolamo, N. E., and Neuman, G.: The Extreme Melt across the Greenland ice sheet in 2012, Geophys. Res. Lett., 39, L20502, doi:10.1029/2012GL053611, 2012.

Overland, J. E., Francis, J. A., Hanna E., and Wang M.: The recent shift in early summer Arctic atmospheric circulation, Geophys. Res. Lett., 39, L19804, doi:10.1029/2012GL053268, 2012

Peltier, W. R.: Global glacial isostasy and the surface of the ice-age earth: the ice-5G (VM2) model and GRACE, Ann. Rev. Earth Pl. Sc., 32, 111–149, doi:10.1146/annurev.earth.32.082503.144359, 2004.

Rae, J. G. L., Aðalgeirsdóttir, G., Edwards, T. L., Fettweis, X., Gregory, J. M., Hewitt, H. T., Lowe, J. A., Lucas-Picher, P., Mottram, R. H., Payne, A. J., Ridley, J. K., Shannon, S. R., van de Berg, W. J., van de Wal, R. S. W., and van den Broeke, M. R.: Greenland ice sheet surface mass balance: evaluating simulations and making projections with regional climate models, The Cryosphere, 6, 1275–1294, doi:10.5194/tc-6-1275-2012, 2012.

Rignot, E., Velicogna, I., van den Broeke, M. R., Monaghan, A., and Lenaerts, J.: Acceleration of the contribution of the Greenland and Antarctic ice sheets to sea level rise, Geophys. Res. Lett., 38, L05503, doi:10.1029/2011GL046583, 2011.

Steffen, K., Nghiem, S. V., Huff, R., and Neumann, G.: The melt anomaly of 2002 on the Greenland ice sheet from active and passive microwave satellite observations, Geophys. Res. Lett., 31, L20402, doi:10.1029/2004GL020444, 2004.

Stroeve, J. C., Box, J. E., and Haran, T.: Evaluation of the MODIS (MOD10A1) daily snow albedo product over the Greenland ice sheet, Remote Sens. Environ., 105, 155–171, 2006.

Swenson, S., Chambers, D., and Wahr, J.: Estimating geocenter variations from a combination of GRACE and ocean model output. J. Geophys. Res., 113, B08410, doi:10.1029/2007JB005338, 2008.

Tapley, B. D., Bettadpur, S., Ries J. C., Thompson, P. F., and Watkins, M. M.: GRACE measurements of mass variability in the Earth system, Science, 305, 503–505, doi:10.1126/science.1099192, 2004.

Tedesco, M.: Snowmelt detection over the Greenland ice sheet from SSM/I brightness temperature daily variations, Geophys. Res. Lett., 34, L02504, doi:10.1029/2006GL028466, 2007.

Tedesco, M.: Assessment and development of snowmelt retrieval algorithms over Antarctica from K-band spaceborne brightness temperature (1979–2008), Remote Sens. Environ., 113, 979–997, 2009.

Tedesco, M. and Fettweis, X.: 21st century projections of surface mass balance changes for major drainage systems of the Greenland ice sheet, Environ. Res. Lett., 7, 045405, doi:10.1088/1748-9326/7/4/045405, 2012.

Tedesco, M., Serreze, M., and Fettweis, X.: Diagnosing the extreme surface melt event over southwestern Greenland in 2007, The Cryosphere, 2, 159–166, doi:10.5194/tc-2-159-2008, 2008.

Tedesco, M., Fettweis, X., van den Broeke, M. R., van de Wal, R. S. W., Smeets, C. J. P. P., van de Berg, W. J., Serreze, M. C., and Box, J. E.: 21st century projections of surface mass balance changes for major drainage systems of the Greenland ice sheet, Environ. Res. Lett., 6, 014005, doi:10.1088/1748-9326/7/4/045405, 2011.

Tedesco, M., Lüthje, M., Steffen, K., Steiner, N., Fettweis, X., Willis, I., Bayou, N., and Banwell, A.: Measurement and modeling of ablation of the bottom of supraglacial lakes in Western Greenland, Geophys. Res. Lett., 39, L02502, doi:10.1029/2011GL049882, 2012.

Thompson, D. W. J. and Wallace, J. M.: The Arctic Oscillation signature in the wintertime geopotential height and temperature fields, Geophys. Res. Lett. 25, 1297–1300, doi:10.1029/98GL00950, 1998.

van den Broeke, M., Bamber, J., Ettema, J., Rignot, E., Schrama, E., van de Berg, W. J., van Meijgaard, E., Velicogna, I., and Wouters, B.: Partitioning recent Greenland mass loss, Science, 326, 984–986, doi:10.1126/science.1178176, 2009.

van der Veen, C. J.: Fracture propagation as means of rapidly transferring surface meltwater to the base of glaciers, Geophys. Res. Lett., 34, L01501, doi:10.1029/2006GL028385, 2007.

Velicogna, I. and Wahr, J.: Significant acceleration of Greenland ice mass loss in spring 2004, Nature, 443, 329–331, doi:10.1038/nature05168, 2006.

Wahr, J., Swenson, S., Zlotnicki, V., and Velicogna, I.: Time-variable gravity from GRACE: first results, Geophys. Res. Lett., 31, L11501, doi:10.1029/2004GL019779, 2004.

Wan, Z. M.: New refinements and validation of the MODIS land-surface temperature/emissivity products, Remote Sens. Environ.,112, 59–74, doi:10.1016/j.rse.2006.06.026, 2008.

Wan, Z. M., Zhang, Y., Zhang, Q., and Li, Z.-L.: Validation of the land-surface temperature products retrieved from terra moderate resolution imaging spectroradiometer data, Remote Sens. Environ., 83, 163–180, 2002.

Wang, D., Morton, D., Masek, J., Wu, A., Nagol, J., Xiong, X., Levy, R., Vermote, E., and Wolfe, R.: Impact of sensor degradation on the MODIS NDVI time series, Remote Sens. Environ., 119, 55–61, 2012.

Weertman, J.: Can a waterfilled crevasse reach the bottom surface of a glacier?, Int. Assoc. Sci. Hydrol. Publ., 95, 139–145, 1973.

Zwally, H. J. and Fiegles, S.: Extent and duration of Antarctic surface melting, J. Glaciol., 40, 46–476, 1994.

Table 1. Melt onset trend in days decade^{-1} for different elevation bands derived from passive microwave data using the approach by Mote and Anderson (1997).

Elevation band	Days decade^{-1}
< 400 m	−11.59 ± 0.015
400–800 m	−9.27 ± 0.010
800–1200 m	−9.83 ± 0.012
1200–1600 m	−7.31 ± 0.012
1600–2000 m	−4.93 ± 0.012
2000–2400 m	−4.49 ± 0.015
2400–2800 m	−2.65 ± 0.015

Table 2. Summer and annual mass changes from GRACE for the period 2003–2012.

Year	Summer mass change (Gt)	Hydrological year	Annual mass change (Gt)
2003	−382.02 ± 119.44	2003–2004	−84.63
2004	−238.57 ± 88.53	2004–2005	−356.16
2005	−419.37 ± 88.53	2005–2006	−133.64
2006	−334.69 ± 88.53	2006–2007	−325.01
2007	−453.90 ± 88.53	2007–2008	−202.42
2008	−345.47 ± 88.53	2008–2009	−218.31
2009	−383.46 ± 88.53	2009–2010	−422.59
2010	−516.27 ± 88.53	2010–2011	−319.00
2011	−435.16 ± 119.44	2011–2012	−574.76
2012	−627.85 ± 88.53		

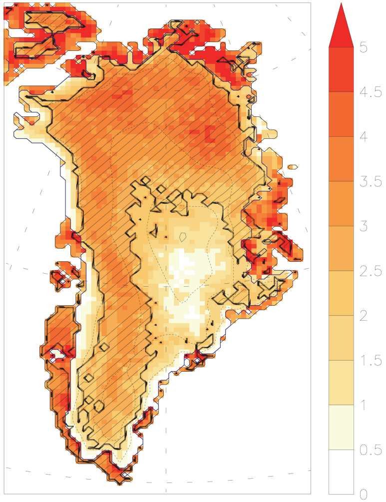

(a) 2012 JJA surface temperature anomaly (K)

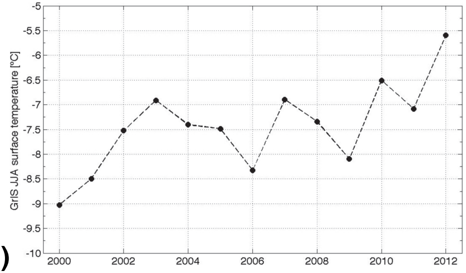

(b)

Fig. 1. (a) 2012 JJA surface temperature anomaly (1958–2011 baseline) simulated by MAR. Hatched areas indicate regions were the anomaly was above two standard deviations from the mean. **(b)** Annual mean surface temperature from MODIS averaged over the entire Greenland ice sheet fort he period 2000–2012.

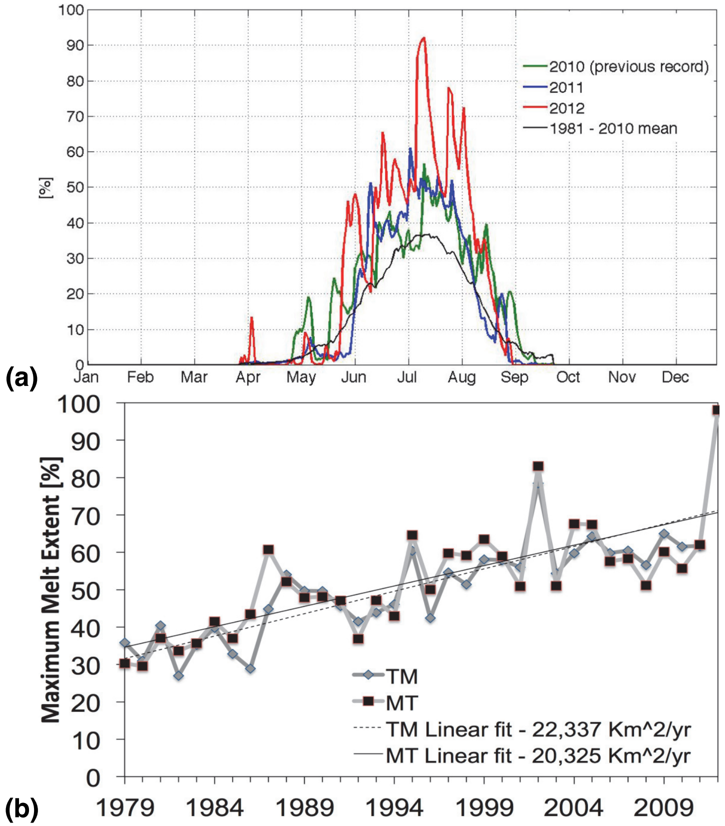

Fig. 2. (a) Melt extent (as a percentage of the Greenland ice sheet) time series derived from spaceborne passive microwave observations using the algorithm in Tedesco (2009) in 2012 (red), in 2011 (blue), 2010 (green, being the previous record) and for the 1981–2010 mean (black). **(b)** Maximum melt extent for the period 1979–2012 using the algorithm in Mote and Anderson (1995), denoted as TM and in Tedesco (2009), denoted as MT.

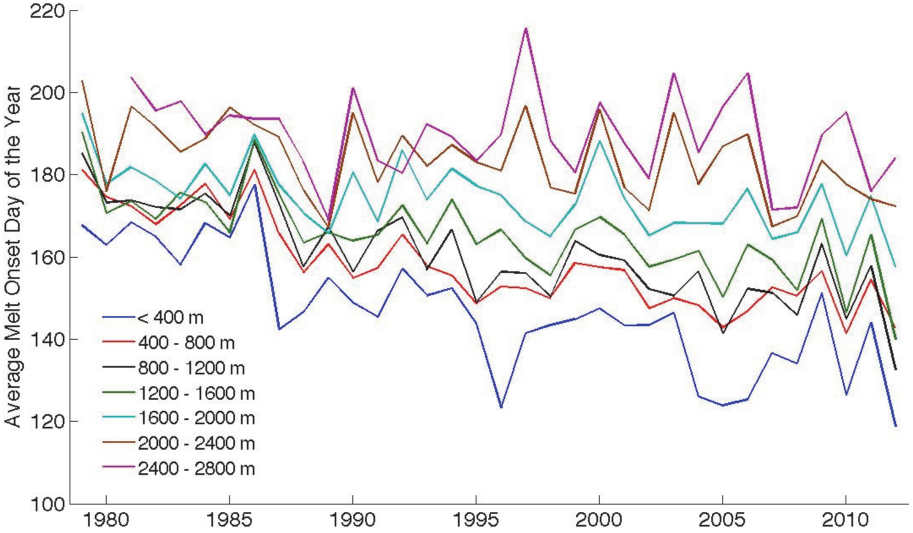

Fig. 3. Average melt onset date (day of year) by elevation bands from passive microwave data using the algorithm in Mote and Anderson (1995).

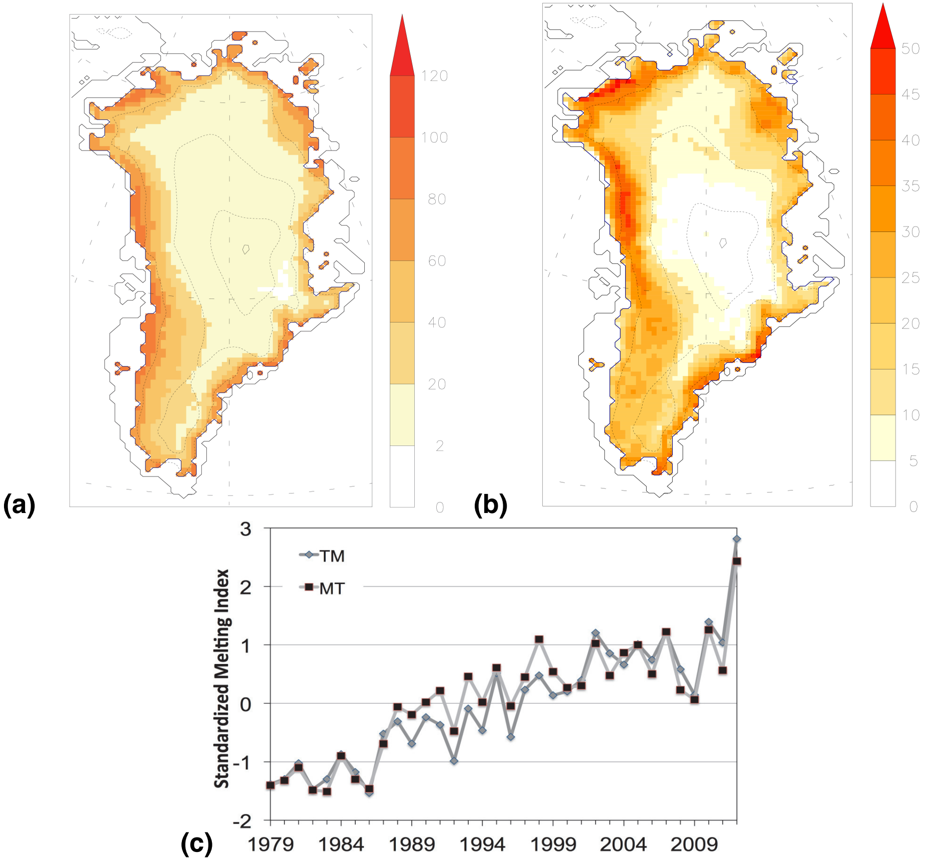

Fig. 4. (a) Melt duration (days) during June, July and August of 2012 from Mote and Anderson (1995) and **(b)** departure from the 1981–2010 average. **(c)** Standardized melting index (SMI) for the period 1979–2012 using the algorithm in Mote and Anderson (1995), denoted as TM and in Tedesco (2009), denoted as MT.

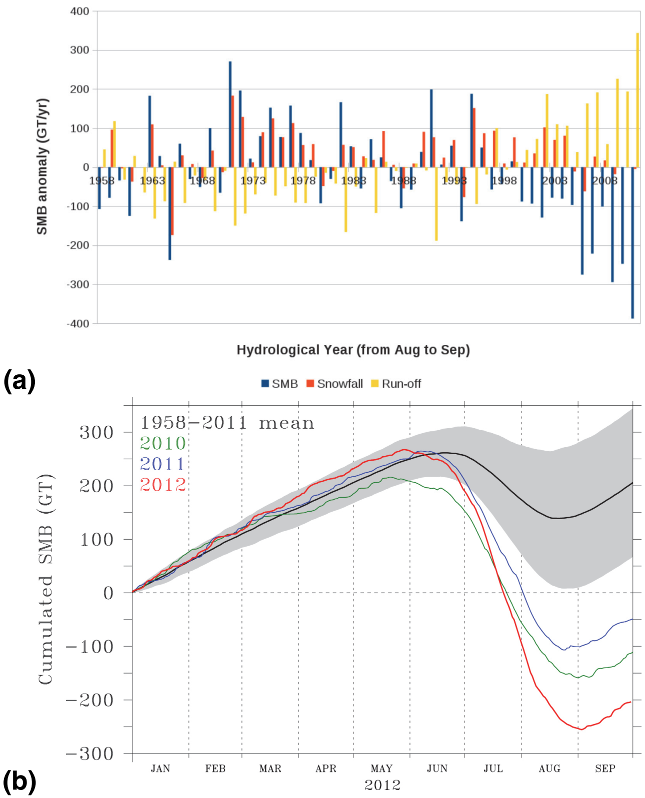

Fig. 5. (a) Barplot of annual time series of the GrIS SMB, snowfall and run-off anomalies integrated over the hydrological year simulated by MAR forced by ERA-40 over 1958–1978 and by ERA-INTERIM over 1979–2012. Units are $\mathrm{Gt\,yr^{-1}}$ and anomalies are given in respect to the 1958–2011 period. **(b)** Daily time series of the cumulative SMB ($\mathrm{Gt\,yr^{-1}}$) using 1st of January as a reference for 2012 (dark blue), 2011 (light red) and 2010 (green) and for the 1958–2011 mean (50 % grey).

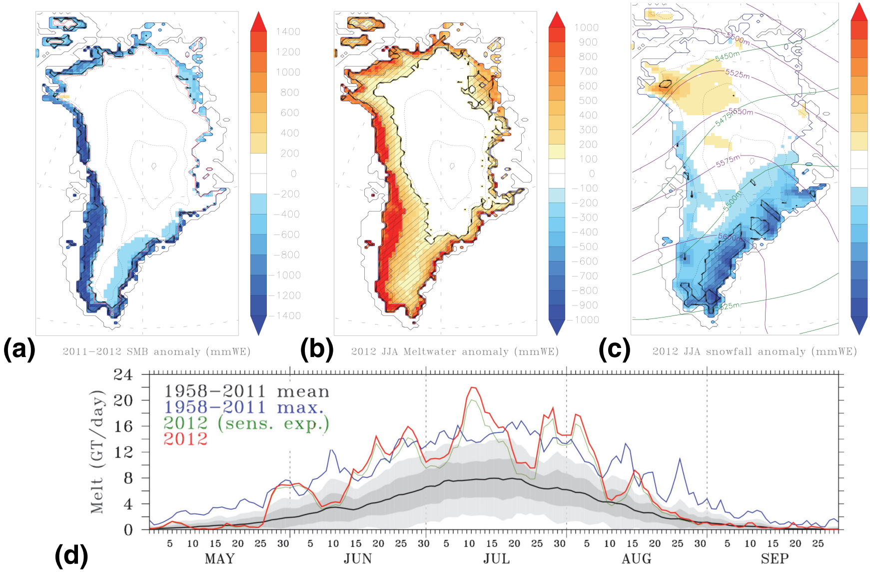

Fig. 6. (a) 2012 anomaly of the SMB integrated over the hydrological year simulated by MAR with respect to 1958–2011. Units are mm WE yr^{-1}. The 2011–2012 ELA (equilibrium line altitude) is plotted as a red line and areas where the anomalies are two times above the 1958–2011 standard deviation of MAR forced by ERA-INTERIM are hatched in black. **(b)** Same as **(a)** but for the JJA melwater production. Only about 40–50 % of this meltwater reaches the ocean by run-off. The ELA is plotted in blue here. **(c)** Same as **(a)** but for the JJA snowfall. **(d)** Time series (in red) of the 2012 GrIS cumulative meltwater production simulated by MAR. The same simulation starting the 1 May 2012 with the state of the snow pack from May 1997 is plotted in green for the purpose of a sensitivity analysis. The 1958–2011 mean simulated by MAR is plotted in black. The dark and light grey areas correspond to the 1958–2011 standard deviation and respectively 2 times the standard deviation of the GrIS MAR simulated values. Finally, the absolute daily maximum values over the considered period are plotted in blue.

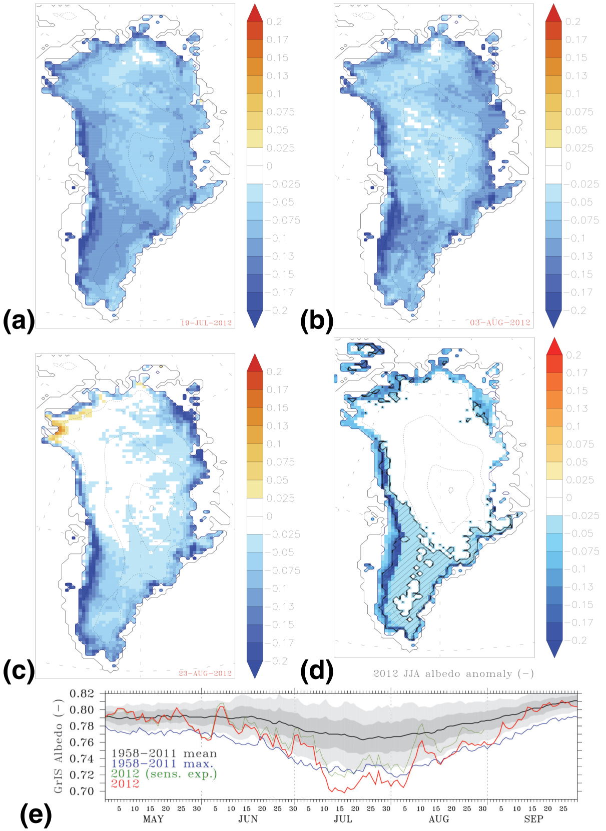

Fig. 7. MODIS Daily albedo anomaly map following Box et al. (2012) for **(a)** 19 July, **(b)** 3 August and **(c)** 23 August, 2012 (using the 2000–2011 mean). MODIS data is re-projected onto MAR grid for graphical consistency purposes. **(d)** JJA MAR albedo anomaly map for 2012 (with respect to the 1958–2011 period). **(e)** Same as Fig. 6d but for albedo.

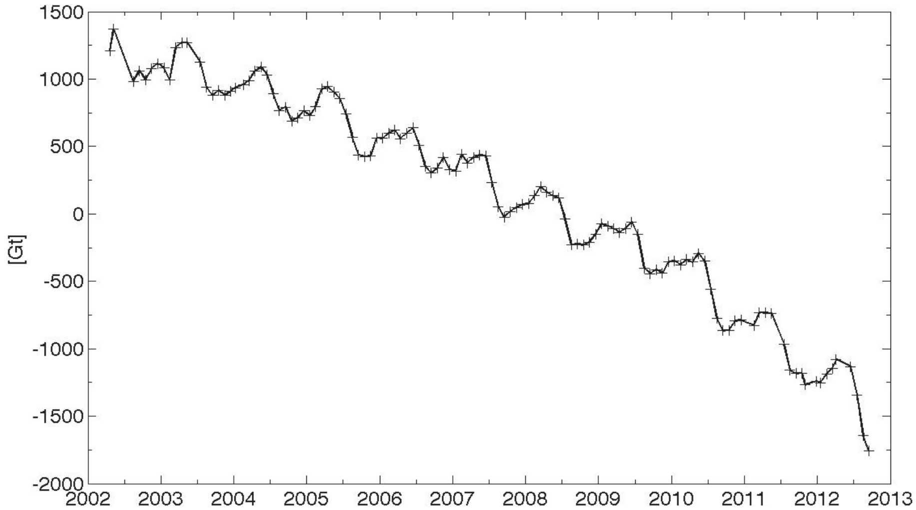

Fig. 8. Cumulative mass anomaly from GRACE updated through September 2012 (Gt).

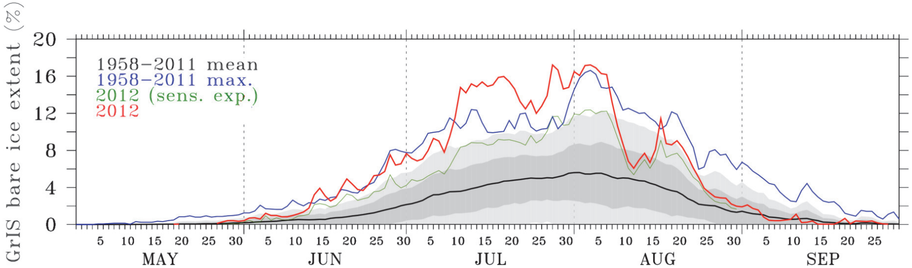

Fig. 9. Same as Fig. 6d but for the daily bare ice extent (where the snow density is higher then 900 kg m^{-3}) in percentage of the GrIS area.

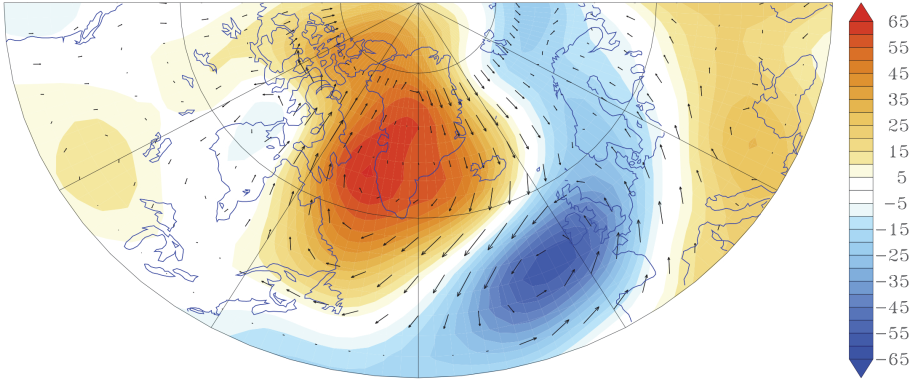

Fig. 10. 700 mb geopotential height (m) and wind anomaly for June, July and August 2012 from the NCEP/NCAR Reanalysis data.

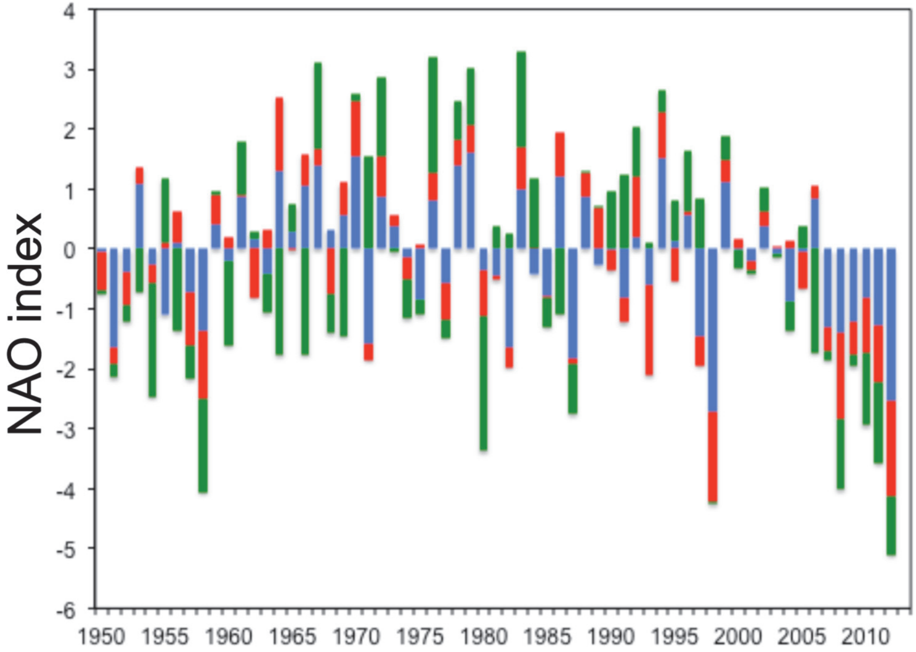

Fig. 11. North Atlantic Oscillation (NAO) index from NOAA climate prediction center for June (blue), July (red), and August (green) for the period 1950–2012.